

Destructive and constructive RIS beamforming in an ISAC-multi-user MIMO network

Steven Rivetti[†], Özlem Tuğfe Demir*, Emil Björnson[†], Mikael Skoglund[†]

[†]School of Electrical Engineering and Computer Science (EECS), KTH Royal Institute of Technology, Sweden

*Department of Electrical-Electronics Engineering, TOBB University of Economics and Technology, Ankara, Türkiye

Abstract—Integrated sensing and communication (ISAC) has already established itself as a promising solution to the spectrum scarcity problem, even more so when paired with a reconfigurable intelligent surface (RIS) as RISs can shape the propagation environment by adjusting their phase-shift coefficients. Albeit the potential performance gain, a RIS also poses a security threat to the system: in this paper, we explore both sides of the RIS presence in a multi-user MIMO (multiple-input multiple-output) ISAC network. We first develop an alternating optimization algorithm, obtaining the active and passive beamforming vectors maximizing the sensing signal-to-noise ratio (SNR) under minimum signal-to-interference-plus-noise ratio (SINR) constraints for the communication users and finite power budget. We also investigate the destructive potential of RIS by devising a RIS phase-shift optimization algorithm that minimizes sensing SNR while preserving the same minimum communication SINR previously guaranteed by the system. We further investigate the impact of the RIS's individual element failures on the system performances. The simulation results show that the RIS performance-boosting potential is as good as its destructive one and that both of our optimization strategies show some resilience towards the investigated impairments.

Index Terms—RIS, malicious RIS, ISAC, MIMO, RIS element failures

I. INTRODUCTION

Reconfigurable intelligent surfaces (RISs) have captured significant interest from both academia and industry for their ability to smartly control challenging radio propagation environments. By using low-cost passive reflecting elements that induce a controllable phase-shift to incoming waveforms, RISs can effectively steer reflected signals towards desired locations while reducing interference at undesired points [1], [2]. Moreover, RISs have recently emerged as a promising technology in integrated sensing and communications (ISAC) applications, increasing the available spatial degrees of freedom. In [3], the sum-rate of the communication user equipments (UEs) is maximized under the worst-case sensing signal-to-noise ratio (SNR) constraint. On the other hand, [4] defines a sensing signal-to-interference-plus-noise ratio (SINR) by taking into account the presence of interfering objects along the sensing path: this sensing SINR is then maximized in a weighted fashion alongside minimizing the communication multi-user interference.

Despite their cost-effective deployment and potential to enhance wireless communication and sensing performance,

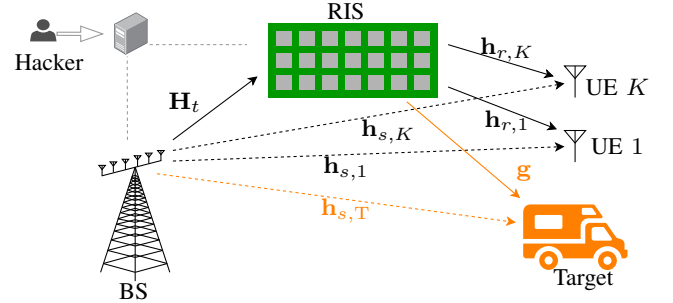


Fig. 1: A RIS-aided ISAC network where a hacker has hacked into the RIS's control circuit.

RISs present critical physical layer security (PLS) challenges. In particular, RISs could potentially be exploited as malicious entities that instead compromise communication and sensing performances. [5] gives an overview of the possible ways in which an illegally deployed RIS can hinder system performance, characterizing signal leakage from the legitimate system to the said RIS and the potential damage of interference attacks launched by the former. The addition of artificial noise onto the legitimate system's transmitted waveform proves to be an effective strategy in increasing the system's PLS, even though the impact of an illegally deployed RIS is still non-negligible. On the other hand, [6] assesses the impact of an active RIS, i.e., a RIS capable of amplifying the impinging signal, onto an Internet of Things network where the RIS aims at minimizing a single device's SNR. Interestingly, the authors analyze both the cases of known and unknown malicious RIS identity.

A significant challenge is that the attacks are difficult to detect because they are not carried out by generating interfering signals, as in traditional jamming. Instead, they involve configuring the RIS to degrade the system's performance. In [7], the impact of these silent attacks is demonstrated, further showing how destructive beamforming is susceptible to channel state information (CSI) uncertainties. An important albeit often overlooked practical consideration about RIS is that individual elements, also known as *pixels*, may fail: [8] gives an overview of the different types of errors that may arise in a practical RIS implementation and characterizes their impact on the RIS radiation pattern. In [9], the authors propose a failure model to specify the amplitude and phase-shift of faulty elements and they propose a diagnostic method.

In this paper, we consider a multi-user (MU)-multiple-input

multiple-output (MIMO) network equipped with an ISAC base station (BS), serving multiple UEs while sensing a target. We first characterize the potential positive impact of a RIS deployment by devising an optimization problem computing active and passive beamforming vectors that maximize the sensing SNR under UEs' SINR constraints and a finite power budget. Inspired by [10], this problem is solved through alternating optimization. We then investigate the RIS destructive potential when, unbeknownst to the BS, the sensing SNR is minimized while the same minimum SINR is still guaranteed to the UEs, as to make this attack harder to detect. We further define a pixel fault model and assess its impact on both optimization algorithms. Numerical simulations show that the RIS is equally capable of boosting and degrading the system performances and the former shows some resilience towards RIS pixel impairments.

Notation: \odot represents the Hadamard (element-wise) product. Boldface lowercase and uppercase letters denote vectors and matrices. The trace of the matrix \mathbf{X} is denoted by $\text{Tr}(\mathbf{X})$. $\text{diag}(\mathbf{x})$ represents the stacking of \mathbf{x} on the main diagonal of a matrix. $[\mathbf{h}]_{n:m}$ represents vector elements comprised between the n -th and m -th ones, denoted by h_n and h_m , of vector \mathbf{h} . The notation $\mathcal{CN}(0, \sigma^2)$ represents the zero-mean circularly symmetric complex Gaussian distribution with variance σ^2 .

II. SYSTEM MODEL

We consider the RIS-assisted MU-MIMO ISAC network shown in Fig. 1, where a BS, equipped with M transmit and M receiving antennas and possessing digital beamforming capabilities, serves K single-antenna UEs in the downlink while sensing the presence of a target. The system is equipped with a RIS made of N reflective elements, whose phase-shifts are described by the vector $\boldsymbol{\theta} = [\theta_1 \dots \theta_N]^\top$, where $|\theta_n| = 1$ for $n = 1, \dots, N$. The static path between the BS and UE k is denoted by $\mathbf{h}_{s,k} \in \mathbb{C}^M$ whereas the static path between the BS and target is denoted by $\mathbf{h}_{s,T} \in \mathbb{C}^M$. The reflected paths are defined in a similar fashion, with $\mathbf{h}_{r,k} \in \mathbb{C}^N$ connecting the RIS and UE k while the target is connected to the RIS via $\mathbf{g} \in \mathbb{C}^N$. Lastly, the BS is connected to the RIS through the channel $\mathbf{H}_t \in \mathbb{C}^{N \times M}$. The end-to-end channel between the BS and UE k is defined as

$$\mathbf{h}_k = \mathbf{h}_{s,k} + \underbrace{\mathbf{H}_t^\text{H} \text{diag}(\boldsymbol{\theta}) \mathbf{h}_{r,k}}_{\triangleq \boldsymbol{\Theta}}. \quad (1)$$

The received signal by UE k can be described by

$$y_k = \sum_{l=1}^L \mathbf{h}_k^\text{H} \mathbf{f}_l t_l + w_k, \quad (2)$$

where $\mathbf{f}_l \in \mathbb{C}^M$ is the precoding vector associated with the l -th stream. We assume that the information meant for UE k is encoded into stream k , while an additional stream $K+1$ is used for sensing purposes. Hence, the total number of streams is $L = K+1$. On the other hand, t_l is the complex-valued unit-power information or sensing symbol and w_k is the complex Gaussian receiver noise with variance σ_k^2 . As for the sensing performance, the two-way sensing channel is

$$\mathbf{H}_T = c_r \underbrace{\mathbf{H}_t^\text{H} \boldsymbol{\Theta} \mathbf{g} \mathbf{g}^\text{H}}_{\triangleq \mathbf{T}} \mathbf{H}_t + c_s \underbrace{\mathbf{h}_{s,T} \mathbf{h}_{s,T}^\text{H}}_{\triangleq \mathbf{H}_{s,T}}. \quad (3)$$

The radar cross section (RCS) associated with the two sensing paths, i.e., the reflected and the static path, are modelled according to the Swerling-I model, that is $c_r \sim \mathcal{CN}(0, \delta_r^2)$ and $c_s \sim \mathcal{CN}(0, \delta_s^2)$. The monostatic sensing observation can be modeled as

$$\mathbf{y}_T = \mathbf{H}_T \mathbf{F} \mathbf{t} + \mathbf{w}_T, \quad (4)$$

where $\mathbf{F} = [\mathbf{f}_1 \dots \mathbf{f}_L]$, $\mathbf{t} = [t_1 \dots t_L]^\top$, and the entries of \mathbf{w}_T are independent and distributed as $\mathcal{CN}(0, \sigma_T^2)$. As for the RIS's pixel malfunctioning, we adopt the *clustered-biased* model defined in [8]: We assume that a set \mathcal{Q} of neighboring pixels assumes a phase-shift that is at a fixed distance κ from the required one. This hardware failure effect can be taken into account by defining a failure mask $\mathbf{m} = [m_1 \dots m_N]^\top$ as [11]

$$m_n = \begin{cases} e^{j\kappa} & \text{if } n \in \mathcal{Q} \\ 1 & \text{otherwise} \end{cases}. \quad (5)$$

The faulty RIS phase-shift vector is then obtained as $\boldsymbol{\theta}^{\text{fault}} = \boldsymbol{\theta} \odot \mathbf{m}$.

III. LEGITIMATE SENSING SNR MAXIMIZATION

The legitimate reason for deploying the RIS is to improve the system performance. Hence, the BS and RIS aim at jointly maximizing the sensing SNR while guaranteeing a minimum SINR to the communication UEs. The sensing SNR can be defined as

$$\rho = \frac{1}{\sigma_T^2} \sum_{l=1}^L \underbrace{\mathbb{E}[\mathbf{f}_l^\text{H} \mathbf{H}_T^\text{H} \mathbf{H}_T \mathbf{f}_l]}_{\rho_l}. \quad (6)$$

Similarly, the SINR of k -th UE is described as

$$\text{SINR}_k(\boldsymbol{\theta}, \mathbf{F}) = \frac{|\mathbf{h}_k^\text{H} \mathbf{f}_k|^2}{\sigma_k^2 + \sum_{l=1, l \neq k}^L |\mathbf{h}_k^\text{H} \mathbf{f}_l|^2}. \quad (7)$$

The sensing SNR maximization problem, solved by the BS under the assumption of a collaborating RIS, is the following:

$$\underset{\boldsymbol{\theta}, \{\mathbf{f}_l\}_{l=1}^L}{\text{maximize}} \quad \frac{1}{\sigma_T^2} \sum_{l=1}^L \rho_l \quad (8a)$$

$$\text{subject to} \quad \text{SINR}_k(\boldsymbol{\theta}, \mathbf{F}) \geq \gamma_k, \quad k = 1, \dots, K, \quad (8b)$$

$$\sum_{l=1}^L \|\mathbf{f}_l\|^2 \leq P, \quad (8c)$$

$$|\theta_n| = 1, \quad n = 1, \dots, N, \quad (8d)$$

where P is the available transmit power of the BS. This problem is evidently non-convex, mainly due to the coupling between the optimization variables and the non-convex unitary modulus constraints. In this section, we will devise an alternating optimization (AO) algorithm, which switches between optimizing the precoding vectors and RIS phase-shifts until convergence.

A. Precoder optimization

In this subsection, we are going to show the first subproblem of the AO algorithm, that is the problem that retrieves the optimal precoder \mathbf{F} while Θ is fixed. It can be shown that the sensing SNR per stream, ρ_l , can be written as $\rho_l = \mathbf{f}_l^H \mathbf{\Gamma} \mathbf{f}_l$, where the matrix $\mathbf{\Gamma}$ is

$$\begin{aligned} \mathbf{\Gamma} = & \delta_s^2 \mathbf{H}_{s,T}^H \mathbf{H}_{s,T} + \delta_m \mathbf{H}_{s,T}^H \mathbf{H}_t^H \Theta \mathbf{T} \Theta^H \mathbf{H}_t \\ & + \delta_m^* \mathbf{H}_t^H \Theta \mathbf{T}^H \Theta^H \mathbf{H}_t \mathbf{H}_{s,T} \\ & + \delta_r^2 \mathbf{H}_t^H \Theta \mathbf{T}^H \Theta^H \mathbf{H}_t \mathbf{H}_t^H \Theta \mathbf{T} \Theta^H \mathbf{H}_t \end{aligned} \quad (9)$$

and $\delta_m = \mathbb{E}[c_r c_s^*]$. By defining the variable $\mathbf{W}_l = \mathbf{f}_l \mathbf{f}_l^H$, we obtain the following problem

$$\text{P1} := \underset{\mathbf{W}_l \succeq 0, \forall l}{\text{maximize}} \quad \frac{1}{\sigma_T^2} \sum_{l=1}^L \text{Tr}(\mathbf{W}_l \mathbf{\Gamma}) \quad (10a)$$

$$\text{subject to } \text{Tr}(\mathbf{W}_k \tilde{\mathbf{H}}_k) \geq \gamma_k \left(\sum_{l \neq k} \text{Tr}(\mathbf{W}_l \tilde{\mathbf{H}}_k) + \sigma_k^2 \right), \quad (10b)$$

$$\sum_{l=1}^L \text{Tr}(\mathbf{W}_l) \leq P, \quad (10c)$$

$$\text{rank}(\mathbf{W}_l) = 1, \quad l = 1, \dots, L, \quad (10d)$$

where $\tilde{\mathbf{H}}_k = \mathbf{h}_k \mathbf{h}_k^H$. We can apply semi-definite relaxation (SDR) to P1 by removing the rank one constraint. The resulting problem becomes convex and can be solved using commercially available solvers like CVX. During our simulations, we have observed that, for the scenario at hand, the optimal solutions $\{\mathbf{W}_l^{\text{opt}}\}_{l=1}^K$ are rank one, thus the relaxation is tight and $\{\mathbf{f}_l^{\text{opt}}\}_{l=1}^K$ can be retrieved through an eigendecomposition. We cannot say the same about \mathbf{W}_L , thus, we employ the *rand C* method from [12], generating a set \mathcal{Z} of randomized solutions that shall be denoted by \mathbf{f}_L^{rd} . We further define the set of feasible randomized solutions as $\mathcal{S} = \{\mathbf{f}_L^{\text{rd}} : \mathbf{f}_L^{\text{rd}} \in \mathcal{Z}, \|\mathbf{f}_L^{\text{rd}}\|^2 \leq P - \sum_{k=1}^K \|\mathbf{f}_k^{\text{opt}}\|^2, \text{ SINR}_k(\theta, \tilde{\mathbf{F}}^{\text{opt}}) \geq \gamma_k, k = 1, \dots, K\}$, where $\tilde{\mathbf{F}}^{\text{opt}} = [\mathbf{f}_1^{\text{opt}} \dots \mathbf{f}_K^{\text{opt}} \mathbf{f}_L^{\text{rd}}]$. The sensing precoding vector is then obtained as

$$\mathbf{f}_L^{\text{opt}} = \arg \max_{\mathbf{f}_L^{\text{rd}} \in \mathcal{S}} \text{Tr}(\mathbf{f}_L^{\text{rd}} (\mathbf{f}_L^{\text{rd}})^H \mathbf{\Gamma}) / \sigma_T^2. \quad (11)$$

B. RIS phase-shift optimization

We now move on to the second part of the AO where we obtain Θ while \mathbf{F} is fixed. We rewrite ρ_l , defined in (6), as

$$\begin{aligned} \rho_l = & \delta_r^2 \text{Tr}(\mathbf{H}_t \mathbf{f}_l \mathbf{f}_l^H \mathbf{H}_t^H \Theta \mathbf{T}^H \Theta^H \mathbf{H}_t \mathbf{H}_t^H \Theta \mathbf{T} \Theta^H) \\ & + 2\Re\left(\text{Tr}\left(\delta_m^* \Theta \mathbf{T}^H \Theta^H \mathbf{H}_t \mathbf{H}_{s,T} \mathbf{f}_l \mathbf{f}_l^H \mathbf{H}_t^H\right)\right) \\ & + \delta_s^2 \text{Tr}(\mathbf{H}_{s,T}^H \mathbf{H}_{s,T} \mathbf{f}_l \mathbf{f}_l^H). \end{aligned} \quad (12)$$

Utilizing the identity $\text{Tr}(\mathbf{A}\mathbf{X}\mathbf{B}\mathbf{X}) = (\text{vec}(\mathbf{X}^T)^T)(\mathbf{B}^T \otimes \mathbf{A})\text{vec}(\mathbf{X})$ and $\mathbf{T} = \mathbf{T}^H$, the first term of ρ_l can be rewritten as

$$\text{vec}(\Theta \mathbf{T} \Theta^H)^H ((\mathbf{H}_t^* \mathbf{H}_t^T) \otimes (\delta_r^2 \mathbf{H}_t \mathbf{f}_l \mathbf{f}_l^H \mathbf{H}_t^H)) \text{vec}(\Theta \mathbf{T} \Theta^H). \quad (13)$$

Then, thanks to the nature of Θ [10] we can write that $\text{vec}(\Theta \mathbf{T} \Theta^H)^H = \text{diag}(\text{vec}(\mathbf{T}))^H \tilde{\Theta}$, where $\tilde{\Theta}$ collects the diagonal entries of $\Theta^* \otimes \Theta$. We can finally rewrite the first term of ρ_l as $\tilde{\Theta}^H \mathbf{Q}_l \tilde{\Theta}$, where

$$\begin{aligned} \mathbf{Q}_l = & (\text{diag}(\text{vec}(\mathbf{T})))^H ((\mathbf{H}_t^* \mathbf{H}_t^T) \otimes (\delta_r^2 \mathbf{H}_t \mathbf{f}_l \mathbf{f}_l^H \mathbf{H}_t^H)) \\ & \times \text{diag}(\text{vec}(\mathbf{T})). \end{aligned} \quad (14)$$

We apply $\text{vec}(\Theta \mathbf{T} \Theta^H)^H = \text{diag}(\text{vec}(\mathbf{T}))^H \tilde{\Theta}$ to the second term of ρ_l as well. Eventually, the sensing SNR per stream, excluding its constant terms, can be further rewritten as

$$\rho_l = \tilde{\Theta}^H \mathbf{Q}_l \tilde{\Theta} + 2\Re(\tilde{\Theta}^H \mathbf{p}_l), \quad (15)$$

where

$$\mathbf{p}_l = \text{diag}(\text{vec}(\mathbf{T}))^H \text{vec}(\delta_m^* \mathbf{H}_t \mathbf{H}_{s,T} \mathbf{f}_l \mathbf{f}_l^H \mathbf{H}_t^H). \quad (16)$$

The RIS phase-shift optimization problem under consideration is non-convex due to the unit-modulus constraints and the objective of maximizing a convex function. To circumvent this issue, we employ the Minorization-Maximization (MM) algorithm to maximize a lower bound on ρ_l [10]. More specifically, we lower-bound $\tilde{\Theta}^H \mathbf{Q}_l \tilde{\Theta}$ by computing its first-order Taylor expansion around the local point $\tilde{\Theta}^{(t)}$:

$$\tilde{\Theta}^H \mathbf{Q}_l \tilde{\Theta} \geq 2\Re(\mathbf{b}_l^{(t)H} \tilde{\Theta}) - \tilde{\Theta}^{(t)H} \mathbf{Q}_l \tilde{\Theta}^{(t)}, \quad (17)$$

where $\mathbf{b}_l^{(t)} = \mathbf{Q}_l \tilde{\Theta}^{(t)}$. Then, ignoring the constant terms, the objective function can be written as

$$\begin{aligned} & \frac{1}{\sigma_T^2} \sum_{l=1}^L 2\Re(\mathbf{b}_l^{(t)H} \tilde{\Theta}) + \Re(\tilde{\Theta}^H \mathbf{p}_l) \\ & = \frac{1}{\sigma_T^2} \sum_{l=1}^L 2\Re(\tilde{\Theta}^H (\Sigma(\mathbf{b}_l^{(t)}) + \Sigma(\mathbf{p}_l)) \tilde{\Theta}), \end{aligned} \quad (18)$$

where $\Sigma(\mathbf{b}_l^{(t)}) \in \mathbb{C}^{N \times N}$ is a matrix built by stacking the elements of $\mathbf{b}_l^{(t)}$. We define the variable $\hat{\Theta} = \tilde{\Theta} \tilde{\Theta}^H$, where $\tilde{\Theta} = [\theta^T, 1]^T$ and $\mathbf{H}_{r,k} = \text{diag}(\mathbf{h}_{r,k})$. Then, the second subproblem of the AO algorithm is

$$\text{P2} := \underset{\hat{\Theta} \succeq 0}{\text{maximize}} \quad \frac{1}{\sigma_T^2} \sum_{l=1}^L 2\text{Tr}(\Xi_l^{(t)} \hat{\Theta}) \quad (19a)$$

$$\text{subject to } [\hat{\Theta}]_{n,n} = 1, \quad n = 1, \dots, N+1, \quad (19b)$$

$$\text{Tr}(\mathbf{R}_{k,k} \hat{\Theta}) \geq \gamma_k \left(\sum_{l \neq k} \text{Tr}(\mathbf{R}_{k,l} \hat{\Theta}) + \sigma_k^2 \right), \quad (19c)$$

$$\text{rank}(\hat{\Theta}) = 1, \quad (19d)$$

where

$$\mathbf{R}_{k,l} = \begin{bmatrix} \mathbf{H}_{r,k}^H \mathbf{H}_t \mathbf{f}_l \mathbf{f}_l^H \mathbf{H}_t^H \mathbf{H}_{r,k} & \mathbf{H}_{r,k}^H \mathbf{H}_t \mathbf{f}_l \mathbf{f}_l^H \mathbf{h}_{s,k} \\ \mathbf{h}_{s,k}^H \mathbf{f}_l \mathbf{f}_l^H \mathbf{H}_t^H \mathbf{H}_{r,k} & |\mathbf{h}_{s,k}^H \mathbf{f}_l|^2 \end{bmatrix}, \quad (20)$$

$$\Xi_l^{(t)} = \begin{bmatrix} \Sigma(\mathbf{b}_l^{(t)}) + \Sigma(\mathbf{p}_l) & \mathbf{0}_{N \times 1} \\ \mathbf{0}_{1 \times N} & 0 \end{bmatrix}. \quad (21)$$

Algorithm 1: Sensing SNR maximizing AO algorithm

- 1: **Initialize:** Randomly generate $\boldsymbol{\theta}^{(0)}$, $t \leftarrow 0$
 - 2: **repeat**
 - 3: Solve the relaxed version of P1 with $\boldsymbol{\theta} = \boldsymbol{\theta}^{(t)}$
 - 4: Retrieve $\mathbf{F}^{(t+1)}$ through Gaussian randomization
 - 5: Solve the relaxed version of P2 with $\mathbf{F} = \mathbf{F}^{(t+1)}$
 - 6: Retrieve $\boldsymbol{\theta}^{(t+1)}$ through Gaussian randomization
 - 7: $t \leftarrow t + 1$
 - 8: **until** $|\rho^{(t)} - \rho^{(t-1)}| \leq \nu$
 - 9: **Output:** $\boldsymbol{\theta}^{\text{opt}}, \mathbf{F}^{\text{opt}}$
-

Once again by removing the rank-one constraints, the relaxed problem becomes convex. Hence, it can be solved by CVX and we can retrieve a good sub-optimal solution via Gaussian randomization. We follow the *rand C* method and generate a set \mathcal{R} of randomized solutions denoted by $\hat{\boldsymbol{\theta}}^{\text{rd}}$. We normalize them as $\boldsymbol{\eta}(\hat{\boldsymbol{\theta}}^{\text{rd}}) = \hat{\boldsymbol{\theta}}^{\text{rd}} / \hat{\theta}_{N+1}^{\text{rd}}$ to ensure that the last element is one and then we define $\tilde{\boldsymbol{\eta}}(\hat{\boldsymbol{\theta}}^{\text{rd}})_n = e^{j\angle \eta(\hat{\boldsymbol{\theta}}^{\text{rd}})_n}$, $n = 1, \dots, N$, to meet the unit modulus constraint. We then define the set of feasible randomized solutions as $\mathcal{E} = \left\{ \tilde{\boldsymbol{\eta}}(\hat{\boldsymbol{\theta}}^{\text{rd}}) : \hat{\boldsymbol{\theta}}^{\text{rd}} \in \mathcal{R}, \text{ SINR}_k(\tilde{\boldsymbol{\eta}}(\hat{\boldsymbol{\theta}}^{\text{rd}}), \mathbf{F}^{\text{opt}}) \geq \gamma_k, k = 1, \dots, K \right\}$, the RIS phase-shifts are recovered as

$$\hat{\boldsymbol{\theta}}^{\text{opt}} = \arg \max_{\tilde{\boldsymbol{\eta}}(\hat{\boldsymbol{\theta}}^{\text{rd}}) \in \mathcal{E}} \frac{2}{\sigma_{\text{T}}^2} \sum_{l=1}^L \text{Tr} \left(\boldsymbol{\Xi}_l^{(t)} \tilde{\boldsymbol{\eta}}(\hat{\boldsymbol{\theta}}^{\text{rd}}) \tilde{\boldsymbol{\eta}}(\hat{\boldsymbol{\theta}}^{\text{rd}})^{\text{H}} \right). \quad (22)$$

The steps of the AO algorithm are outlined in Algorithm 1.

IV. MALICIOUS RIS SENSING SNR DEGRADATION

As mentioned in the introduction, we assume that the RIS control circuit has been hacked. The hacker aims at degrading the sensing SNR so that the sensing target can go undetected. Furthermore, to make the hacker's action hard to detect, the UEs are still guaranteed a minimum SINR. Motivated by the collaboration between the BS and RIS, we assume that the hacker has access to the optimal precoders \mathbf{F}^{opt} . Additionally, we consider the worst-case scenario in which perfect CSI is available to the hacker. Hence, the hacker models the cascaded channel as $\mathbf{h}_k = \mathbf{h}_{s,k} + \mathbf{H}_t^{\text{H}} \mathbf{H}_{r,k} \boldsymbol{\theta}$. According to these assumptions, the sensing SNR per stream can be rewritten as

$$\rho_l = \delta_r^2 \left| \mathbf{f}_l^{\text{H}} \mathbf{H}_t^{\text{H}} \mathbf{G} \boldsymbol{\theta} \right|^2 \left\| \mathbf{H}_t^{\text{H}} \mathbf{G} \boldsymbol{\theta} \right\|^2 + \boldsymbol{\theta}^{\text{H}} \mathbf{M}_l \boldsymbol{\theta} + \delta_s^2 \mathbf{f}_l^{\text{H}} \mathbf{H}_{s,\text{T}}^{\text{H}} \mathbf{H}_{s,\text{T}} \mathbf{f}_l, \quad (23)$$

where

$$\mathbf{G} = \text{diag}(\mathbf{g}), \quad (24)$$

$$\mathbf{M}_l = \mathbf{G}^{\text{H}} \mathbf{H}_t \left(\delta_m^* \mathbf{H}_{s,\text{T}} \mathbf{f}_l \mathbf{f}_l^{\text{H}} + \delta_m \mathbf{f}_l \mathbf{f}_l^{\text{H}} \mathbf{H}_{s,\text{T}}^{\text{H}} \right) \mathbf{H}_t^{\text{H}} \mathbf{G}. \quad (25)$$

The sensing-degrading selection of $\boldsymbol{\Theta}$ is obtained by solving the problem

$$\text{P3} := \underset{\boldsymbol{\theta}}{\text{minimize}} \quad \frac{1}{\sigma_{\text{T}}^2} \sum_{l=1}^L \rho_l \quad (26a)$$

$$\text{subject to } \text{SINR}_k(\boldsymbol{\theta}, \mathbf{F}^{\text{opt}}) \geq \gamma_k, \quad k = 1, \dots, K, \quad (26b)$$

$$|\theta_n| = 1, \quad n = 1, \dots, N. \quad (26c)$$

This problem is non-convex and therefore challenging to solve. However, we will demonstrate that each non-convex term of the objective function can be reformulated in a manageable manner, enabling us to solve P3 using the convex-concave procedure (CCP) [13]. The first term of ρ_l is the product between individually convex terms of $\boldsymbol{\theta}$. We decouple those terms by introducing the variables $\mathbf{s} = [s_1 \dots s_L]^{\text{T}}$ and r , redefining ρ_l by removing the constant term as

$$\rho_l = \delta_r^2 s_l^2 r^2 + \boldsymbol{\theta}^{\text{H}} \mathbf{M}_l \boldsymbol{\theta} \quad (27)$$

and adding the constraints

$$|\mathbf{f}_l^{\text{H}} \mathbf{H}_t^{\text{H}} \mathbf{G} \boldsymbol{\theta}|^2 \leq s_l^2, \quad l = 1, \dots, L, \quad (28)$$

$$\left\| \mathbf{H}_t^{\text{H}} \mathbf{G} \boldsymbol{\theta} \right\|^2 \leq r^2. \quad (29)$$

The product between s_l^2 and r^2 is still nonconvex, thus, we rewrite it by leveraging the square-completion method:

$$\rho_l = \frac{\delta_r}{2} (s_l^2 + r^2)^2 - \frac{\delta_r}{2} s_l^4 - \frac{\delta_r}{2} r^4 + \boldsymbol{\theta}^{\text{H}} \mathbf{M}_l \boldsymbol{\theta}. \quad (30)$$

The last term is a source of non-convexity because, albeit Hermitian symmetric, \mathbf{M}_l is not necessarily positive semi-definite (PSD). We then introduce the auxiliary variables $\boldsymbol{\alpha} = [\alpha_1 \dots \alpha_L]^{\text{T}}$ and redefine ρ_l as

$$\rho_l = \frac{\delta_r}{2} (s_l^2 + r^2)^2 - \frac{\delta_r}{2} s_l^4 - \frac{\delta_r}{2} r^4 + \alpha_l \quad (31)$$

with the additional constraints

$$\hat{\boldsymbol{\theta}}^{\text{H}} \underbrace{\begin{bmatrix} \mathbf{M}_l & \mathbf{0}_{N \times 1} \\ \mathbf{0}_{1 \times N} & 0 \end{bmatrix}}_{\mathbf{M}_l} \hat{\boldsymbol{\theta}} \leq \alpha_l, \quad (32)$$

where $\hat{\boldsymbol{\theta}} = [\boldsymbol{\theta}^{\text{T}}, 1]^{\text{T}}$. We then apply the CCP method [13] to (32) and obtain

$$\begin{aligned} & \hat{\boldsymbol{\theta}}^{\text{H}} \hat{\mathbf{M}}_l^{(+)} \hat{\boldsymbol{\theta}} + 2\Re \left(\hat{\boldsymbol{\theta}}^{(t)\text{H}} \hat{\mathbf{M}}_l^{(-)} \hat{\boldsymbol{\theta}} \right) \leq \alpha_l \\ & + \hat{\boldsymbol{\theta}}^{(t)\text{H}} \hat{\mathbf{M}}_l^{(-)} \hat{\boldsymbol{\theta}}^{(t)}, \quad l = 1, \dots, L, \end{aligned} \quad (33)$$

where $\hat{\mathbf{M}}_l^{(+)}, \hat{\mathbf{M}}_l^{(-)}$ are respectively the positive and negative semi-definite parts of $\hat{\mathbf{M}}_l$ and $\hat{\boldsymbol{\theta}}^{(t)}$ being a local point. The second and third term of (30) are concave and are then locally upper bounded by their first-order Taylor expansion. We define an approximated version of ρ_l around the local point $(\mathbf{s}^{(t)}, r^{(t)}, \hat{\boldsymbol{\theta}}^{(t)})$ (by also removing the constant terms):

$$\tilde{\rho}_l^{(t)} = \frac{\delta_r}{2} (s_l^2 + r^2)^2 - 2\delta_r s_l^{(t),3} s_l - 2\delta_r r^{(t),3} r + \alpha_l. \quad (34)$$

Algorithm 2: Sensing SNR minimization algorithm

- 1: **Initialize:** Set $t = 0$ and $\lambda^{(0)}$, randomly generate $\theta^{(0)}$,
 $s_l^{(0)} = \left| \mathbf{f}_l^H \mathbf{H}_t^H \mathbf{G} \theta^{(0)} \right|^2$, $r^{(0)} = \left\| \mathbf{H}_t^H \mathbf{G} \theta^{(0)} \right\|^2$
 - 2: **repeat**
 - 3: Retrieve $(\mathbf{s}^{(t+1)}, r^{(t+1)}, \hat{\theta}^{(t+1)})$ by solving P4
 - 4: $\lambda^{(t+1)} = \min(\mu \lambda^{(t)}, \lambda_{\max})$
 - 5: $t \leftarrow t + 1$
 - 6: **until** $\left\| \theta^{(t)} - \theta^{(t-1)} \right\| \leq \nu$, $\|\xi\| \leq \nu$, $\|\mathbf{v}\| \leq \nu$
 - 7: **Output:** θ^{opt}
-

The feasible-point pursuit successive convex approximation procedure [14] is applied to (26c), decoupling it into

$$\left| \hat{\theta}_n \right|^2 \leq 1 + \xi_n, \quad n = 1, \dots, N, \quad (35a)$$

$$\left| \hat{\theta}_n^{(t)} \right|^2 - 2\Re(\hat{\theta}_n^* \hat{\theta}_n^{(t)}) \leq \xi_{N+n} - 1, \quad n = 1, \dots, N, \quad (35b)$$

where $\xi = [\xi_1 \dots \xi_{2N}]^\top$ is a vector of auxiliary variables. The minimum SINR constraint (26b) is written as:

$$\gamma_k \left(\hat{\theta}^H \mathbf{U}_k \hat{\theta} + \sigma_k^2 \right) - \hat{\theta}^H \mathbf{R}_{k,k} \hat{\theta} \leq 0 \quad (36)$$

where

$$\mathbf{U}_k = \begin{bmatrix} \mathbf{H}_{r,k}^H \mathbf{H}_t \mathbf{F}_{-k} \mathbf{F}_{-k}^H \mathbf{H}_{r,k}^H & \mathbf{H}_{r,k}^H \mathbf{H}_t \mathbf{F}_{-k} \mathbf{F}_{-k}^H \mathbf{h}_{s,k} \\ \mathbf{h}_{s,k}^H \mathbf{F}_{-k} \mathbf{F}_{-k}^H \mathbf{H}_t \mathbf{H}_{r,k} & \mathbf{h}_{s,k}^H \mathbf{F}_{-k} \mathbf{F}_{-k}^H \mathbf{h}_{s,k} \end{bmatrix}. \quad (37)$$

The notation $\mathbf{F}_{-k} \in \mathbb{C}^{M \times L-1}$ indicates a matrix containing all the precoding vectors except the one assigned to the k -th UE. (36) is then convexified as

$$\begin{aligned} & \gamma_k \left(\hat{\theta}^H \mathbf{U}_k \hat{\theta} + \sigma_k^2 \right) - 2\Re(\hat{\theta}^{(t)H} \mathbf{R}_{k,k} \hat{\theta}) \\ & + \hat{\theta}^{(t)H} \mathbf{R}_{k,k} \hat{\theta}^{(t)} \leq v_k, \quad k = 1, \dots, K, \end{aligned} \quad (38)$$

where $\mathbf{v} = [v_1 \dots v_K]^\top$ are slack variables. Lastly, (28) and (29) are locally approximated as

$$|\tau_l \hat{\theta}|^2 + s_l^{(t),2} - 2s_l^{(t)} s_l \leq 0, \quad l = 1, \dots, L, \quad (39)$$

$$\|\hat{\mathbf{H}} \hat{\theta}\|^2 + r^{(t),2} - 2r^{(t)} r \leq 0, \quad (40)$$

where $\tau_l = [\mathbf{f}_l^H \mathbf{H}_t^H \mathbf{G}, 0]$ and $\hat{\mathbf{H}} = [\mathbf{H}_t^H \mathbf{G}, \mathbf{0}_{M \times 1}]$. We are now finally able to define the convex reformulation of P3:

$$\text{P4} := \underset{\hat{\theta}, \mathbf{v}, \xi, \mathbf{s}, r}{\text{minimize}} \quad \frac{1}{\sigma_T^2} \sum_{l=1}^L \tilde{\rho}_l^{(t)} + \lambda^{(t)} (\|\xi\| + \|\mathbf{v}\|) \quad (41a)$$

$$\text{subject to } \hat{\theta}_{N+1} = 1, \quad (41b)$$

$$(33), (35), (38), (39), (40), \quad (41c)$$

$$\xi, \mathbf{v}, \mathbf{s}, r \geq 0, \quad (41d)$$

where $\lambda^{(t)}$ is a penalty factor adjusting the impact of the auxiliary variables onto the optimization function. The iterative procedure is described in Algorithm 2, with ν being a preset tolerance level.

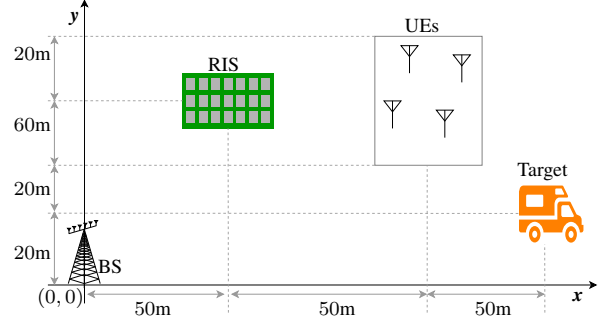


Fig. 2: Illustration of the simulation setup.

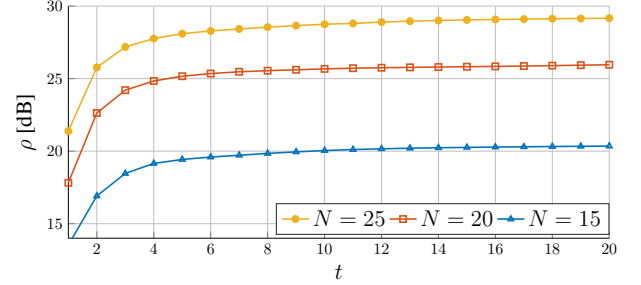


Fig. 3: Alg. 1 ρ maximization vs t for different values of N .

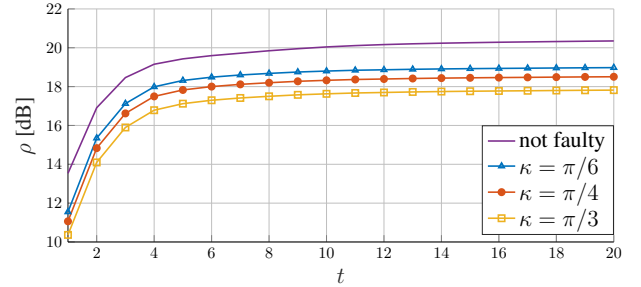


Fig. 4: Alg. 1 ρ maximization vs t in presence of failures.

V. NUMERICAL RESULTS

The simulation results are averaged over 500 independent channel realizations with $|\mathcal{Z}| = |\mathcal{R}| = 1000$. The number of BS antennas is $M = 30$ and the number of UEs is $K = 4$ and, unless otherwise specified, $N = 15$, with a number of faulty pixels equal to $|\mathcal{Q}| = 4$. The static paths $\mathbf{h}_{s,k}$, $\mathbf{h}_{s,T}$, and \mathbf{g} are independent and identically distributed (i.i.d.) Rician fading with a K-factor of 10 whereas \mathbf{H}_t is a scattering-free line of sight (LoS) channel. Lastly, $\mathbf{h}_{r,k}$ are i.i.d Rayleigh fading. The static and reflected path RCS variances are set to $\delta_r^2 = \delta_s^2 = 10^{-5}$ whereas $\delta_m = 9 \cdot 10^{-6}$. We assume an equal minimum SINR for all UEs, denoted by γ and, unless otherwise specified, it is equal to 2. The BS available power is 3dB and the UEs and sensing noise variances are set to $\sigma_k^2 = \sigma_T^2 = 1$. We consider the 2D area shown in Fig. 2, where the UEs are randomly distributed within the highlighted area.

A. Sensing SNR maximization

We have first tested the sensing SNR maximization capabilities of Algorithm 1. Fig. 3 shows that ρ is a monotonically in-

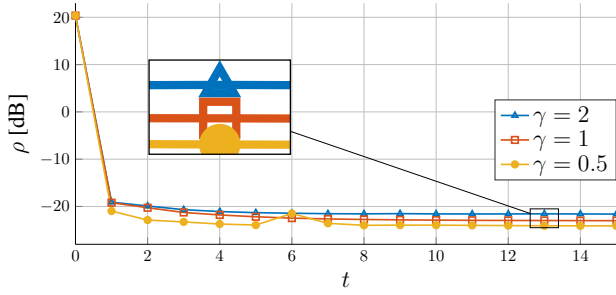


Fig. 5: Alg. 2 ρ minimization vs t for different values of γ .

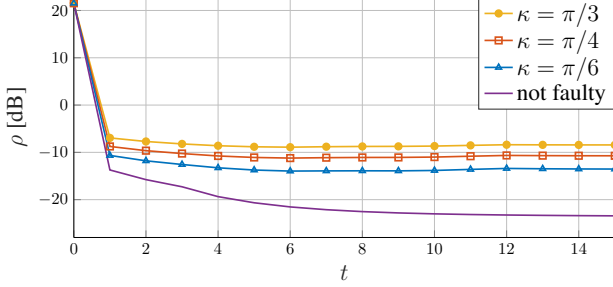


Fig. 6: Alg. 2 ρ minimization vs. t in the presence of failures.

creasing function of the number of iterations t and convergence is reached in 20 iterations. Unsurprisingly, a larger RIS size allows us to reflect more energy towards the target, resulting in a higher ρ . There are diminishing returns in increasing N : when N goes from 15 to 20, the final value of ρ increases by 5 dB whereas when N goes from 20 to 25 the increase is halved. Fig. 3 shows the impact of clustered pixel failures [8] onto Algorithm 1: We notice that this kind of failure does not alter the maximization trend, but leads to convergence to a lower ρ -value. For example, a big phase bias magnitude of $\pi/3$ attains a ρ value only 2 dB lower than the one obtained with a perfectly functioning RIS, giving our algorithm a certain degree of resilience.

B. Malicious RIS action

Fig. 5 shows how Algorithm 2 causes SNR reduction. One iteration is sufficient to obtain a 40 dB SNR reduction. This reduction further increases in the span of 15 iterations, reaching a final value around -22 dB. Such an attack is particularly complicated to detect as the communication SINRs are untouched, thus the communication UEs will not see any difference in their service. A reduction of γ would improve the SNR reduction at the expenses of a higher vulnerability to detection. However, a 50% reduction in γ corresponds to a mere 2 dB SNR reduction. Furthermore, setting γ to 0.5 gives rise to an SNR that's 1 dB lower than the one obtained with an $\gamma = 1$. We attribute the bump at iteration 6 of the SNR curve with $\gamma = 0.5$ to an outlying realization amongst the averaged ones: it is worth mentioning that said bump does not hinder the SNR convergence process and ρ at iteration 15 is lower than ρ at iteration 5. Fig. 6 assesses the impact of clustered RIS pixel failures onto Algorithm 2's ρ minimization action. Contrary to what we observed in Fig. 4, faulty RIS hardware has a bigger impact onto the final sensing SNR. A phase-shift

bias of $\pi/6$ is sufficient to induce a 10 dB penalty onto the final value of ρ , making this algorithm much less resilient than the previous one.

VI. CONCLUSIONS

We have investigated the potential of a RIS in an ISAC MU-MIMO network. The positive side of the RIS's presence has been investigated by devising an optimization algorithm maximizing the sensing target SNR under the communication SINR constraints and a finite power budget. The negative side arises when a hacker takes control of the RIS, computing its phase-shifts to minimize the target SNR, under the same SINR constraints. The hacker can make the sensing target practically invisible to the system. We have further taken into account the presence of clustered pixel failures affecting the RIS. Numerical simulations have exemplified how great both potentials are and how the RIS element impairments impact them based on the RIS intentions.

REFERENCES

- [1] G. C. Alexandropoulos, N. Shlezinger, and P. Del Hougne, "Reconfigurable intelligent surfaces for rich scattering wireless communications: Recent experiments, challenges, and opportunities," *IEEE Communications Magazine*, vol. 59, no. 6, pp. 28–34, 2021.
- [2] K. Chen, C. Qi, O. A. Dobre, and G. Y. Li, "Simultaneous beam training and target sensing in ISAC systems with RIS," *IEEE Transactions on Wireless Communications*, 2023.
- [3] R. Liu, M. Li, and A. L. Swindlehurst, "Joint beamforming and reflection design for RIS-assisted ISAC systems," in *2022 30th European Signal Processing Conference (EUSIPCO)*. IEEE, 2022, pp. 997–1001.
- [4] K. Zhong, J. Hu, C. Pan, M. Deng, and J. Fang, "Joint waveform and beamforming design for RIS-aided ISAC systems," *IEEE Signal Processing Letters*, vol. 30, pp. 165–169, 2023.
- [5] Y. Wang, H. Lu, D. Zhao, Y. Deng, and A. Nallanathan, "Wireless communication in the presence of illegal reconfigurable intelligent surface: Signal leakage and interference attack," *IEEE Wireless Communications*, vol. 29, no. 3, pp. 131–138, 2022.
- [6] Z. Lin, H. Niu, K. An, Y. Hu, D. Li, J. Wang, and N. Al-Dahir, "Pain without gain: Destructive beamforming from a malicious RIS perspective in IoT networks," *IEEE Internet of Things Journal*, 2023.
- [7] S. Rivetti, Ö. T. Demir, E. Björnson, and M. Skoglund, "Malicious reconfigurable intelligent surfaces: How impactful can destructive beamforming be?" *arXiv preprint arXiv:2402.13351*, 2024.
- [8] H. Taghvaei, A. Cabellos-Aparicio, J. Georgiou, and S. Abadal, "Error analysis of programmable metasurfaces for beam steering," *IEEE Journal on Emerging and Selected Topics in Circuits and Systems*, vol. 10, no. 1, pp. 62–74, 2020.
- [9] J. Zhang, X. Hu, and C. Zhong, "Phase calibration for intelligent reflecting surfaces assisted millimeter wave communications," *IEEE Transactions on Signal Processing*, vol. 70, pp. 1026–1040, 2022.
- [10] Z.-M. Jiang, M. Rihan, P. Zhang, L. Huang, Q. Deng, J. Zhang, and E. M. Mohamed, "Intelligent reflecting surface aided dual-function radar and communication system," *IEEE Systems Journal*, vol. 16, no. 1, pp. 475–486, 2021.
- [11] C. Ozturk, M. F. Keskin, V. Sciancalepore, H. Wymeersch, and S. Gezici, "RIS-aided localization under pixel failures," *IEEE Transactions on Wireless Communications*, 2024.
- [12] Z.-Q. Luo, J. F. Sturm, and S. Zhang, "Multivariate nonnegative quadratic mappings," *SIAM Journal on Optimization*, vol. 14, no. 4, pp. 1140–1162, 2004.
- [13] G. Zhou, C. Pan, H. Ren, K. Wang, M. Di Renzo, and A. Nallanathan, "Robust beamforming design for intelligent reflecting surface aided MISO communication systems," *IEEE Wireless Communications Letters*, vol. 9, no. 10, pp. 1658–1662, 2020.
- [14] O. Mehanna, K. Huang, B. Gopalakrishnan, A. Konar, and N. D. Sidiropoulos, "Feasible point pursuit and successive approximation of non-convex qcqp," *IEEE Signal Processing Letters*, vol. 22, no. 7, pp. 804–808, 2014.